Ultrasonics Sonochemistry 71 (2021) 105386

Contents lists available at ScienceDirect

Ultrasonics Sonochemistry

journal homepage: www.elsevier.com/locate/ultson

Design and optimization of a cavitating device for Congo red decolorization: Experimental investigation and CFD simulation

Zahra Abbas-Shiroodi, Mohammad-Taghi Sadeghi *, Soroush Baradaran

School of Chemical, Oil and Gas Engineering, Iran University of Science and Technology (IUST), Tehran, Iran

ARTICLE INFO

Keywords:
Hydrodynamic cavitation
Circular Venturi
Cavitation zone
RSM
CFD

ABSTRACT

The aim of this work is to perform design and optimization of a cavitating device based on CFD simulation. A set of operational and geometrical parameters such as convergence angle, divergence angle, length of throat, and inlet pressure that can affect the hydrodynamic cavitation phenomenon generating in a Venturi are evaluated through CFD simulation and experimental approaches. Response surface methodology (RSM) was employed to achieve the optimum geometrical configuration. The CFD results show that the maximum cavitation zone in the Venturi can be obtained when half angle of the convergence section, throat length and half angle of the divergence section are 22.7°, 4 mm, and 6.5°, respectively. A maximum decolorization of 38.8% has been obtained using the designed Venturi at cavitation number (Cv) of 0.12. Additionally, the results were compared to that of various orifice plates. A decolorization of 26.2% using 33 holes orifice plate and 11.55% in one hole orifice plate approved the superiority of the designed Venturi.

1. Introduction

Hydrodynamic Cavitation (HC) is a phenomenon resulting from generation, growth, and collapse of micro-bubbles at a small time interval (milliseconds). This can release a large amount of energy and subsequently, the cavities are formed and grow in size, until reaching into a certain level [1]. Based on the reactor hydrodynamic and geometric specification, the cavitation phenomenon can promote temperature and pressure in the order of 1000 to 5000 K and 100 to 5000 Pa, respectively [2]. Moreover, HC generates the conditions of high energy density with very high local temperatures and pressures in the liquid medium [3]. Chemical effects are expected based on the pyrolysis of molecules leading to the generation of free radicals following to presence of HC and collapse of bubbles that generate the extreme energy. This capability has made the HC applicable to a widely used process for oxidation based treatments and degradation of various organic pollutants [4], sludge treatment [5], removal of pharmaceuticals (clofibric acid, ibuprofen, ketoprofen, naproxen, diclofenac, carbamazepine) [6], toxic cyanobacteria (Microcystis aeruginosa) [7], bacteria (Legionella pneumophila) [8] and viruses (Rotavirus) [9] from water and wastewater [10]. The degradation is stimulated when HC is combined with other techniques such as various advanced oxidation processes (AOP) [4,11]. The phenomenon can also be utilized for more novel applications such as hydrodynamic cavitation assisted Oxidative Desulfurization (HCAOD) process [12,13]. Several researchers studied the degradation of Reactive Red 120 dye [14], Coomassie Brilliant Blue [15], Congo red [16], reactive orange 4 dye [17], imidacloprid [18], commercial pesticide [19], degradation of Acid Red 88 dye [20] were used the same dimensions of Venturi.

Congo red is azoic dye with two azo bonds (—N═N—) chromophores in its molecular structure which widely utilizes in the textile and plastic industries [21,22]. The release of this dye from textile effluent leads to severe impacts in the aquatic ecosystem and human beings due to the toxic, carcinogenic, and mutagenic effects [23,24]. These dye effluents are highly colored, have complex chemical structure, high molecular weight, high solubility in water, and persistence one is discharged into the natural environment [25]. Many studies have been done to reduce the dangerous effects of the dye. Khadhraoui et al. [25] investigated the degradation of the Congo red in aqueous solutions using ozone. The extent of TOC removal was about 32%. Schmidt et al [22] studied the biodegradation of Congo red that 93.6% decolorization was reported within 120 h.

HC solely can be generated by introducing constrictions, such as an orifice plate [26], Venturi [17], or throttling valve also using a stator and rotor [27], swirling jet-induced reactor [28]. Mancuso et al. [29] compared the cavitation generated at multiple orifice plates with a

* Corresponding author.
E-mail address: sadeghi@iust.ac.ir (M.-T. Sadeghi).

https://doi.org/10.1016/j.ultsonch.2020.105386
Received 30 December 2019; Received in revised form 6 October 2020; Accepted 29 October 2020
Available online 13 November 2020

modified swirling jet-induced reactor (Ecowirl). At similar operative condition (p = 2 bar), the higher degradation obtained using Ecowirl reactor (15%) rather than orifice plate (9%) as well as this study shows that HC reactors are more energy efficient and cavitational yields as compared to the acoustic cavitation.

Saharan et al. [30] examined the effect of geometry and operating parameters of different cavitating devices, namely circular Venturi, slit Venturi, and single hole orifice plate in the degradation of Orange-G dye. The optimized inlet pressure was 3 bar (cavitation number = 0.29) for the slit Venturi and 5 bar for the circular Venturi (cavitation number = 0.15) and orifice plate (cavitation number = 0.24) respectively. About 92% decolorization was observed in the case of slit Venturi, whereas 76% and 45% decolorization was reported with circular Venturi and orifice plate respectively within 2 h at optimized inlet pressure.

Pardhan and Gogate [31] investigated the effectiveness of degradation of p-nitrophenol by means of a Venturi tube and orifice plate that compared them. At the same operating pressure (5.7 psi), the liquid velocity in the Venturi tube (10.15 m/s) is higher than in the orifice plate (7.54 m/s) therefore, the number of passes through the cavitation zone increase in the Venturi and the operating cavitation number is lower in the case of Venturi (1.57) as compared to orifice (3.43). The extent of removal was 53.4% and 51% for Venturi and orifice respectively. In their study, the author attributed the Venturi tube generates much lower turbulence intensity and lower pressure loss due to smooth variation of convergence and divergence sections in comparison with orifice plate. Similar results were obtained by Badve et al. [32] who disinfected seawater using a circular Venturi, a rectangular slit Venturi and an orifice plate.

Bashir et al. [33] studied on five designs of throat Venturi (circular, slit, annular ring, annular slit and double annular slit) using CFD simulation. The double annular slit Venturi exhibited the largest cavitation zone area as well as highest intensity of collapse of cavities. The slit Venturi, in which the slit length is equal to its height (1:1) with a half angle of divergence section 5.5°, was reported as the best geometry in order to get a high cavitational activity. It is important to study different geometries because of based on the geometrical configuration of the caviting system is possible to achieve different values of the extent of degradation. The effect of different geometries can be investigated using Computational Fluid Dynamic (CFD) analysis. Mancuso at el. [34] reported results of numerical simulations were in good agreement with experimental data. Hence, their results demonstrated that numerical methods are impressive in obtaining magnitudes of significant operational and geometrical parameters affecting the performance of the cavitating device [35,36].

In this work, the effect of different geometrical and operational parameters is investigated to obtain the optimum values of a cavitating device in order to be verified in decolorization of Congo red. For this purpose, Response Surface Methodology (RSM) was applied by means of CFD simulation. In the previous literatures, there are not more study on changing the Venturi geometries and validating the numerical prediction using experimental in terms of geometric parameters. Most of the studies were focused on the degradation of different pollutants using single or multiple hole orifice plates and synergetic effect of hydrodynamic cavitation and other additives. Generally, the only effect of the two parameters namely the half outlet divergence angle and the length of the throat is investigated. The effect of ratio of diameter to length of throat has been simulated only in a several specified ratios, such as 1:1, 1:2, and 1:3. Hence, angles such as 5.5, 6.5, and 7.5 are also generally used to evaluate the effect of the divergence angle without there is no reason to choose these values. In addition to these two parameters, the role of the half inlet convergence angle is studied in this work. The RSM enables assessment of the mutual interaction of geometric parameters as well as the significance of each parameter and the number of different states of the Venturi dimension. So far, no study has been carried out to report the interaction of geometrical parameters of circular Venturi. The interaction between geometrical parameters is demonstrated by response contour plots. Moreover, the simulated cavitation zone is validated by experimental tests. Eventually, the optimal Venturi performance is evaluated experimentally in comparison with various orifice geometries with same β both individually.

2. Modeling methodology

2.1. RSM design

Venturi is consisted of a converging section, a throat, and a diverging section. Geometric parameters such as the convergence angle, divergence angle and length of throat play substantial role in the state of cavitation region. The Response Surface Methodology (RSM) is used to determine the optimal geometry objected to provide the highest overall intensity of HC. Box-Behnken Design (BBD) of RSM has the capability to analyze and model relations between the independent parameters and response by means of regression model equation. Hence, it can specify the interactive effect of different variables [10,11]. In order to perform the assessment, convergence angle (A), length of the throat (B) and divergence angle (C) are considered as the three main variables. These independent variables and their levels are shown in Table 1. Operating conditions such as temperature and inlet pressure in all simulations are assumed to be the same.

Table 2 shows the suggested geometries by the Box-Behnken design (BBD). Accordingly, 15 simulations were required that included three replicates of the central run.

Following the simulation, in order to obtain the highest extent of the HC, surface area of the absolute pressure graph in terms of distance was considered as the response. At lower surface area under the graph, where pressure is equal to the vapor pressure of the fluid, cavitation zone is larger and more vapor is produced. All geometries were compared in the same operational condition, i.e. inlet pressure 6 bar, flow rate 20 lit/min and vapor pressure 3540 Pa. The inlet diameter and throat diameter were 30 mm and 4 mm respectively. Results of each simulation were applied to fit a quadratic prediction correlation for the response.

2.2. Numerical method

The first step in analysis of the axisymmetric, incompressible, viscous and homogeneous fluid is to use Navier-stokes equation. The incompressible flow assumption seems reasonable since the inverse of the speed of sound squared is very low. Continuity and momentum equations are the governing equations of the fluid flow. A two-phase fluid flow through the Venturi, inclusive of bulk liquid and vapor inside the cavities is considered. Hence, the multiphase mixture approach is employed for the simulation. A separate set of governing equation is applied for each phase. The governing equation and momentum equation for the mixture can be expressed respectively as:

The continuity equation for the mixture could be written as Eq. (1) [37]:

$$\frac{\partial \rho_{mix}}{\partial t} + \vec{\nabla}(\rho_{mix}\vec{v_{mix}}) = 0 \quad (1)$$

where $\vec{v}_{mix}$ is the mass-averaged velocity and is calculated based on Eq. (2):

Table 1
Range and factor level of process variables.

Factors	Symbol code	Range and Levels		
		1−	0	1+
Convergence angle	A	°20.7	°22.7	°24.7
Length of throat (mm)	B	8	4	0
Divergence angle	C	°5	°6.5	°8

Table 2
Designed geometries using the Box-Behnken method.

Run	Inlet angle	Outlet angle	L (mm)
1	22.7	8	8
2	20.7	8	4
3	24.7	8	4
4	24.7	6.5	0
5	22.7	6.5	4
6	22.7	6.5	4
7	22.7	6.5	4
8	20.7	6.5	8
9	24.7	6.5	8
10	22.7	8	0
11	22.7	5	8
12	24.7	5	4
13	22.7	5	0
14	20.7	5	4
15	20.7	6.5	0

$$\overrightarrow{\nu}_{mix} = \frac{\sum_{k=1}^{n} \alpha_k \rho_k \overrightarrow{\nu}_k}{\rho_{mix}} \tag{2}$$

α_k is the volume fraction of phase k, n is the number of phases and ρ_{mix} is the density of the mixture as Eq. (3):

$$\rho_{mix} = \sum_{k=1}^{n} \alpha_k \rho_k \tag{3}$$

Additionally, the momentum equation for the mixture could be considered as Eq. (4):

$$\frac{\partial}{\partial t}\left(\rho_{mix}\overrightarrow{\nu}_{mix}\right) + \nabla\cdot\left(\rho_{mix}\overrightarrow{\nu}_{mix}\overrightarrow{\nu}_{mix}\right) = -\nabla p + \nabla\cdot[(\mu_{mix}+\mu_t)(\nabla\overrightarrow{\nu}_{mix} + \nabla\overrightarrow{\nu}^{T}_{mix})] \tag{4}$$

where μ_{mix} is the viscosity of the mixture according to Eq. (5):

$$\mu_{mix} = \sum_{k=1}^{n} \alpha_k \mu_k \tag{5}$$

Mass transfer between the two liquids and vapor in the cavitation is obtained by Eq. (6):

$$\frac{\partial}{\partial t}(\rho_{mix} f) + \nabla(\rho_{mix}\vec{v}_v f) = \nabla(\gamma\nabla f) + R_e + R_c \tag{6}$$

where f, $\vec{v}$, and γ represent vapour mass fraction, vapor phase velocity and effective exchange coefficient, respectively. Hence, R_e and R_c are the vapourisation rate and condensation rate. The rate of phase change are based on Rayleigh-Plesset equation as Eqs. (7),(8) [38]:

$$\text{Where } p < psat \; R_e = C_e \frac{V_{ch}}{\sigma}\rho_l\rho_v\sqrt{\frac{2(P_v - P)}{3\rho_l}}(1-f) \tag{7}$$

$$\text{Where } p > psat \; R_c = C_c \frac{V_{ch}}{\sigma}\rho_l\rho_l\sqrt{\frac{2(P - P_v)}{3\rho_l}}f \tag{8}$$

where parameters v_{ch}, σ and p_v are the characteristic velocity, surface tension coefficient and vapour pressure, respectively. v_{ch} is approximated via the local turbulence intensity (i.e., $v_{ch} = \sqrt{k}$). C_e*and*C_c are empirical constants corresponding to 0.02 and 0.01, respectively.

Moreover, the effects of turbulence on cavitation account by threshold pressure phase change that is obtained by Eq. (9):

$$P_v = (P_{sat} + \frac{P'_{turb}}{2}) \tag{9}$$

P'_{turb} is the turbulent pressure fluctuation given as Eq. (10):

$$P'_{turb} = 0.39\rho k \tag{10}$$

where k is the turbulent kinetic energy [39].

2.3. CFD model

In order to investigate the effect of parameters on the extent of HC, CFD technique is employed. Governing and momentum equations were discretized using control volume scheme. Steady state cavitation with no slip velocity near the wall was considered for the analysis. The Schnerr-Sauer model is applied and simulated using a mixture model for multi-phase flow. In this model the vapor and liquid phases are considered as interpenetrating continuum. k-ε scheme was considered for the turbulence model standard. Density, momentum, vapor and turbulent kinetic energy as well as turbulent dissipation rate are discretized using the first order upwind discretization scheme. Pressure–velocity coupling was utilized by SIMPLEC algorithm and the residual for continuity equation was set at 10^{-6}. Simulations were carried out at the fixed outlet pressure of 1 atm.

CFD simulation results are highly affected by mesh size. In order to investigate the grid independency, two other grids with 310,460 and 2,497,572 cells were generated. The plot of absolute pressure variable along the Venturi using three different mesh sizes is shown in Fig. 1. Effect of grid resolution on the absolute pressure for three different mesh types have been compared and the grid with 1,745,750 cells is used in the numerical simulation.

3. Experimental

3.1. Chemicals

Congo red (CR) dye (molecular formula: $C_{32}H_{22}N_6O_6S_2Na_2C_{32}H_{22}N_6O_6S_2Na_2$) and ferrous sulphate heptahydrate ($FeSO_4{\cdot}7H_2O$, 98%) was obtained from SAMCHUN Co., Korea. Solution pH was adjusted using NaOH and H_2SO_4 that were purchased from SAMCHUN and MERK, respectively. Commercial grade hydrogen peroxide (50% wt.) was also used. The solution of CR was prepared in tap water for all experiments.

3.2. Experimental setup and procedure

Hydrodynamic cavitation reactor setup is shown in Fig. 2. The setup includes a holding tank, pump of power rating 5.5 kW, control valves (V1, V2, V3 and V4), flow meter, and pressure gauges. The bottom of the

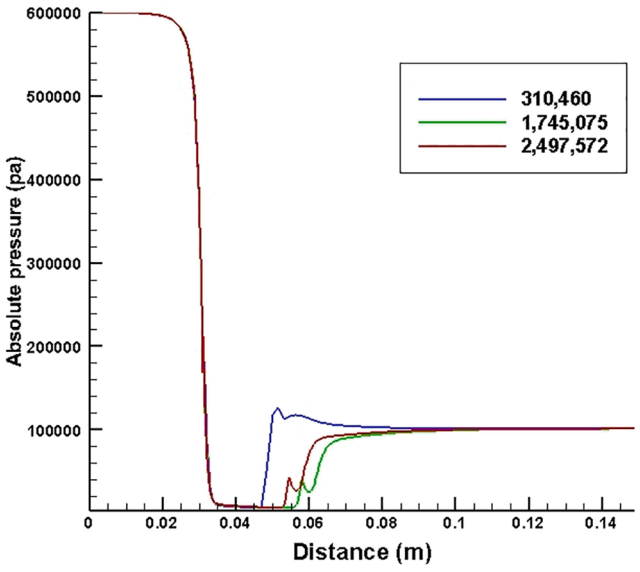

Fig. 1. Absolute pressure profile of venturi in three different mesh sizes.

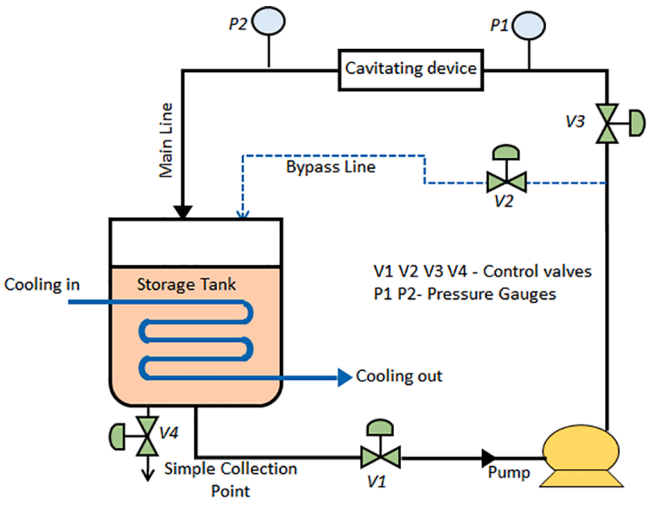

Fig. 2. Schematic diagram of hydrodynamic cavitation reactor set-up.

holding tank is connected to the suction side of the pump and the flow is pumped into two lines; the main line and the bypass line. Pressure and flow of liquid in the cavitating device can be controlled via the bypass flow. In order to avoid any air induction, the main line and the bypass line are terminated inside the tank below the solution level. The two pressure gauges are installed upstream and downstream which measure the fluid pressures. Four manual valves are provided at appropriate places to control the flow through the lines. The tank is equipped with a cooling coil to maintain temperature. Experiments were carried out in the presence of a cavitating device (Venturi and orifice plate) placed in main lines. Fig. 3 shows the schematic of Venturi and orifice plates used in this work. Four types of orifice plates as shown in Fig. 3 are compared with Venturi tube. Details of the cavitating devices are shown in Table 3.

Decolorization of Congo red (CR) has been carried out using various HC reactors at different conditions with a fixed aqueous Congo red (CR)

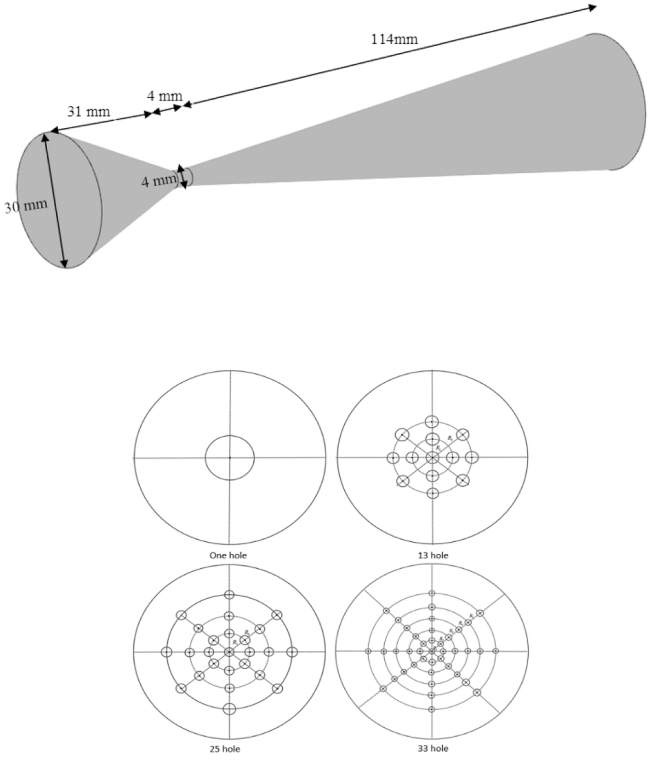

Fig. 3. Schematics of venturi and orifice plate devices

Table 3
Details of the cavitating devices.

Cavitating device	Number of holes	Diameter of holes (mm)	Perimeter of holes (mm)	α (mm^{-1})
OP1	1	4	12.56	1
OP2	13	1.1	44.9	3.64
OP3	25	0.8	62.8	5
OP4	33	0.69	71.5	5.8
Venturi	1	4	12.56	1

solution of 10 L volume. The holding tank was filled with an aqueous solution of the pollution. Initial concentration of Congo red (CR) was kept constant at 20 ppm in all experiments. A reaction time was considered as 60 min and samples for analysis were collected at regular interval of time. The temperature of the solution during experiments was kept constant in all cases at 33 ± 3 ℃ by circulating water through the cooling coil in the tank. The HC inlet pressure was optimized by varying in the range of 4–7 bar for getting maximum possible decolorization of Congo red (CR) via different cavitating devices.

3.3. Analysis

The samples of aqueous phase were analyzed on UV-spectrometer (PG T80 +) and a change in the absorption of CR with time at the maximum wavelength of 485 nm observe. The absorbance of CR reduces with increasing treatment time through the hydrodynamic cavitation device. The Concentration of Congo red (CR) was determined based on the calibration curve. This calibration curve was obtained using the standard CR solutions with different concentration over the range 5–30 ppm and measuring the absorbance of the standard solutions. The relationship between absorption and concentration based on calibration curve is presented in Eq. (11):

$$concentration = -89.326*(absorption^2) + 94.856*(absorption) + 0.4467 \quad (11)$$

Then, the extent of decolorization of CR was characterized by the Eq. (12):

$$Decolorization\ rate\ (\%) = \frac{C_0 - C_t}{C_0}*100 \quad (12)$$

where $C_0(mgL^{-1})$ and C_t (mgL^{-1}) are the concentration of initial time and action time, respectively.

4. Results & discussion

4.1. Response surface analysis of the geometric parameters of venturi

The effect of geometric variables is determined by CFD simulation and Response Surface Methodology. As stated before, Response surface methodology (RSM) is applied for modeling, analysis and evaluation of the interaction effects of different geometrical variables. Box–Behnken design as a subset of the response surface methodology (RSM) is employed for evaluation of the simulation results and addressing the optimum geometry of Venturi. Results of all the runs are reflected in Table 4.

In order to validate the proposed model, analysis of variance can be used. ANOVA results for the response are presented in Table 5. The analysis implied significance of the model. The F-Value for a factor is a measure for the evaluation of the variance related to the factor and the residual variance. In other words, the mean square of the factor divided by the mean square of the residual. Moreover, P-values emphasize the model from the statistical point of view. The pattern of interactions between the parameters can be realized using the P-value and F-value. Generally, large Fisher's value (F-value) and small Probability value (P-value) would indicate the statistical significance of the model. The F-

Table 4
Box–Behnken design for geometry optimization and modelling results.

Run	Inlet angle	Outlet angle	L	Area
1	22.7	8	8	25575.2
2	20.7	8	4	26545.3
3	24.7	8	4	25993.6
4	24.7	6.5	0	25094.2
5	22.7	6.5	4	20,581
6	22.7	6.5	4	20,581
7	22.7	6.5	4	20,581
8	20.7	6.5	8	25053.4
9	24.7	6.5	8	25108.1
10	22.7	8	0	26645.7
11	22.7	5	8	26999.6
12	24.7	5	4	27180.9
13	22.7	5	0	27,565
14	20.7	5	4	27916.2
15	20.7	6.5	0	26816.5

value of the model is equals to 1928.64 and P-value is less than 0.0001 that demonstrates the model terms are significant [17,21]. The model parameters including A, B, C, and interaction of AC, BC, A^2, B^2, C^2 are significant model terms that have a P-value lower than 0.05. Besides, as can be observed in Table 4, "lack of fit F-value" (13.19) is not significant.

The value of R^2 (coefficient of determination) is 0.9956, which indicates that the proposed quadratic correlation fits and data very well. In other words, only less than 1% of the total variation did not fit the model. The behavior of effective factors on the response (R) that is the area of cavitation region can be modeled by the Eq. (13):

$$(R)^{0.23} = +9.82 - -0.033*A - -0.055*B - -0.039*C + 3.574E - 003*AB + 0.041*AC - -0.012*BC + 0.26*A^2 + 0.37*B^2 + 0.24*C^2 \quad (13)$$

In this equation, response is the surface area below the graph of absolute pressure in terms of distance. A, B, C are convergence angle, length of the throat, and divergence angle, respectively. The value of the coefficient in each term of the correlation show increasing and decreasing effects of the parameters on the response. According to the coefficients of the correlation, the parameter B (divergence angle) is the most effective parameter that affect cavitation zone. The shape of the divergent section prevents early cavity collapse as well as the divergence angle strongly affects the pressure profile and the pressure recovery rate in the cavitation zone whereas the convergence angle and length of the throat have a limited effect on it. Parameter A (convergence angle) is less significant than the other parameters since the convergence angle affect the vapor fraction at throat and rate of pressure drop in the convergence section. Generally, angle of convergence at the inlet of the Venturi could be effectively utilized to control the cavity growth whereas angle of divergence of the exit controls the collapse of cavity.

Interaction between parameters and the response at three-dimensional response surface is shown in Fig. 4. The figure relates divergence angle and convergence angle with the response. Pressure recovery rate is controlled by the angle of divergence [40]. Accordingly, it could be concluded that disproportionate increase or decrease of divergence angle results in decreasing cavitation zone. At higher angle, pressure recovers immediately and cavities don't reach their maximum size and collepse rapidly. However, pressure recovery and intensity of the collapse increase due to boundary layer separation and sudden collapse of the cavities. On the other hand, for the small divergent angle, pressure recovery occurs smoothly. Therefore, cavity will grow to attain the maximum size prior to collapse. Higher length of cavitation zone was obtained in optimum divergence angle [39].

Fig. 4.b relates the divergence angle and length of throat with the response. Residence time of cavity in the throat also contributes to the maximum size cavities before collapse. Effect of the residence time is determined by the height to length ratio. At higher length, increasing the length of throat, enhances the distance that the fluid has to pass in throat. Consequently, the throat velocity decreases and cavitation number increases limiting the overall intensity of HC. Hence, the residence time of the bubbles decreases in an area where the pressure is equal to the vapor pressure of the fluid and the bubbles do not grow to their maximum size. On the other hand, at lower length, velocity decreases due to cavities quick move from converging section to diverging section leading to boundary layer separation that takes place at leading edge of the throat. Due to the higher residence time, bubbles collides with other bubbles or decrease their diameter due to collisions with unsolved gases. Hence, an optimum range of throat length exists for maximum extent of HC. This finding is also in accordance with feature researches [41].

4.2. Performance validation of optimized simulated venturi

Based on the RSM result, the optimum value of parameters are found to be convergence angle of 22.7°, divergence angle of 6.5° and throat length of 4 mm. The absolute pressure countor and pressure profile of the optimum geometry using CFD is shown in Fig. 5. The inlet pressure and vapor pressure are assumed equal to 6 bar and 3540 Pa, respectively.

In order to evaluate the performance of Venturi, cavitation length is compared to experimental section. Pressure contour of the optimized Venturi in experimental conditions i.e. optimum inlet pressure of 5 bar and temperature of 36℃ is shown in Fig. 6. The pressure contour has been matched with imaging evidence of cavitation zone forming in Venturi. Fig. 7 shows image of cavitation zone in the downstream of Venturi.

4.3. Effect of HC inlet pressure

Inlet pressure and flow rate are the most important operational parameters that affect the cavitational process. Influence of the inlet pressure was studied in the range of 4 bar to 10 bar via CFD simulation. Outlet pressure was assumed to be 1 bar. The velocity of the throat and

Table 5
ANOVA results and statistical parameters.

Source	Sum of Squares	df	Mean Square	F-value	p-value Prob > F	
Model	0.88	9	0.098	1928.64	< 0.0001	Significant
A-inlet angle	8.952E-003	1	8.952E-003	176.57	< 0.0001	
B-outlet angle	0.024	1	0.024	476.00	< 0.0001	
C-L	0.012	1	0.012	234.54	< 0.0001	
AB	5.108E-005	1	5.108E-005	1.01	0.3616	
AC	6.665E-003	1	6.665E-003	131.30	< 0.0001	
BC	5.730E-004	1	5.730E-004	11.29	0.0201	
A^2	0.24	1	0.24	4823.68	< 0.0001	
B^2	0.49	1	0.49	9709.41	< 0.0001	
C^2	0.21	1	0.21	4135.27	< 0.0001	
Residual	2.535E-004	5	5.070E-005			
Lack of Fit	2.413E-004	3	8.043E-005	13.19	0.0713	not significant

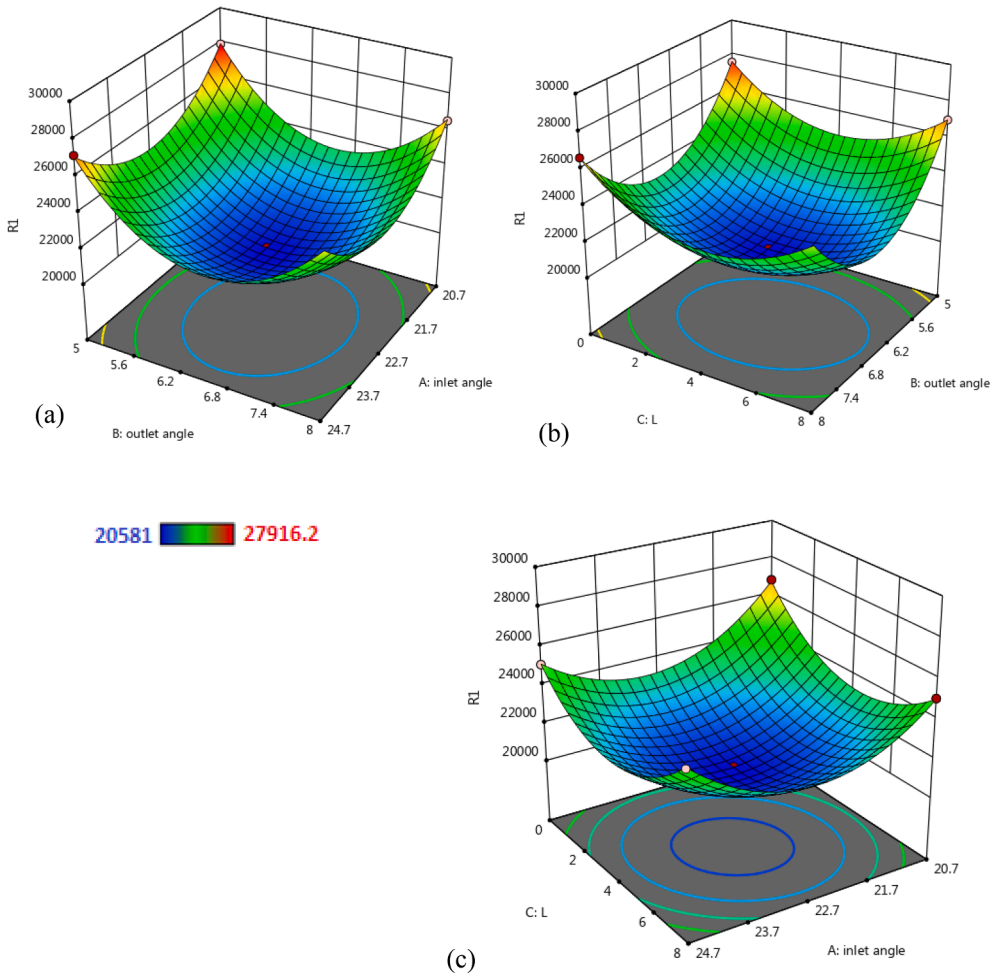

Fig. 4. Response surface plots of the R1as a function of: (a) inlet angle and outlet angle, (b) outlet angle and L, (c) inlet angle and L at P = 6 Bar and P_{sat} = 3540 Pa.

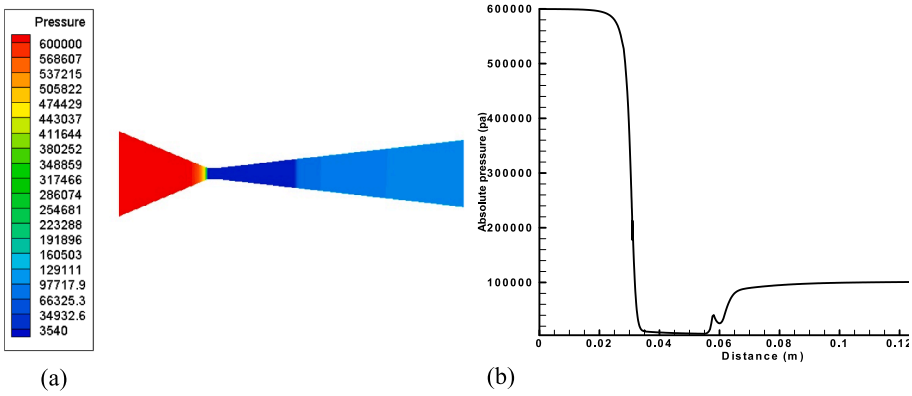

Fig. 5. a) Pressure contour of optimized venturi, b) Pressure profile of optimized venturi.

cavitation number has been given in Table 6 for each inlet pressure which is used to investigation of hydraulic characteristics of the circular Venturi. The C_v can be defined as Eq. (14):

$$C_V = \frac{P_2 - P_v}{\frac{1}{2}\rho v_0^2} \tag{14}$$

where P_2 is the fully recovered downstream pressure, P_v is the vapor pressure of the liquid and v_0 is the velocity of the throat. In low pressure region and ideal condition, the lower the cavitation number, i.e. $C_v < 1$, the better it is for cavity generation. But, cavities may also be generated at the cavitation number greater than 1 because of the presence of dissolved gases. Based on studies, lower cavitation number, i.e. between 0.1 and 0.3, is better for wastewater treatment application [41]. Simulation results and pressure contours at different HC inlet pressures are depicted in Fig. 8. The results indicate that increasing the HC inlet pressure, highly promotes the cavitation zone length. In our study, an inlet pressure as 10 bar gives maximum cavitational zone. It occurs due to dramatic increase in the velocity of throat. As can be seen in the Table 6, cavitation number decreases that leads to producing greater

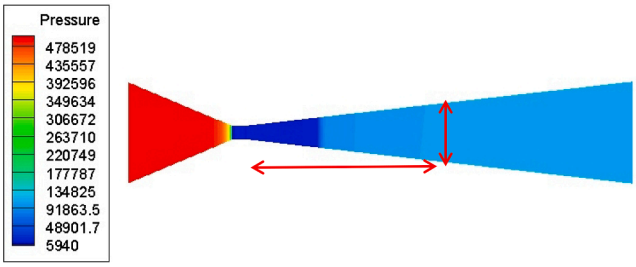

Fig. 6. Pressure contour of venturi in experimental condition.

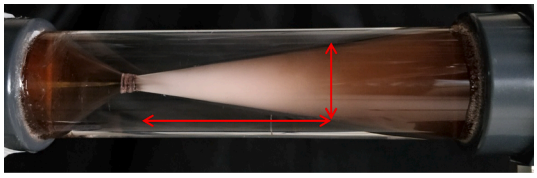

Fig. 7. Image of cavitation zone in the downstream of venturi.

Table 6
C_v for different inlet pressures at optimized Venturi.

Pressure (bar)	Velocity (m/s)	C_v
4	37.14	0.14
5	39.8	0.12
6	42.44	0.10
7	45.09	0.094

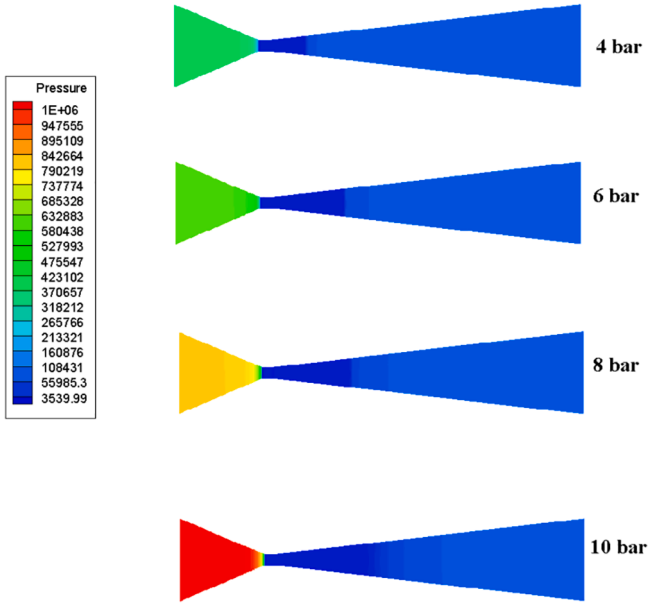

Fig. 8. Pressure contour at different inlet gauge pressure.

number of cavities. Excessive decay of the cavitation number leads to super cavitation process. In this situation, vast number of cavities are formed and downstream section gets covered by the cavity cloud [42,43]. Therefore, Venturi should always be operated above choked cavitation conditions.

Effect of pressure was investigated experimentally leading to maximum CR decolorization of 38.8% in 60 min at 5 bar inlet pressure. Fig. 9 shows the extent of decolorization of Congo red at various inlet pressure. Decolorization rate decreases with further increase in inlet

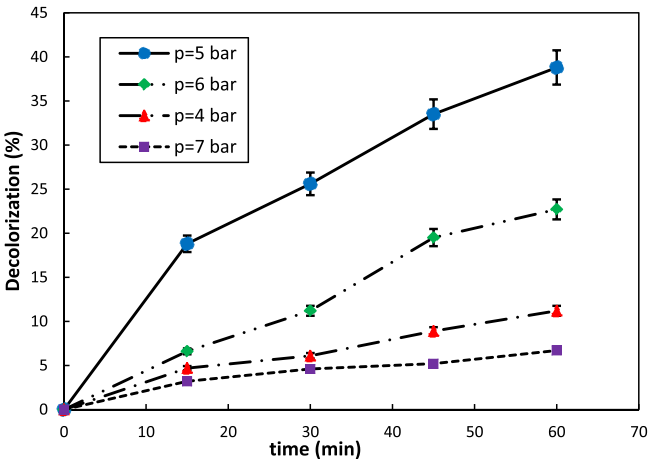

Fig. 9. Effect of inlet pressure on the rate of decolorization of Congo red (Initial concentration of Congo red 20 ppm, temperature 35℃).

pressure exceeding the optimum value. The decay in decolorization extent, could be attributed to the presence of super cavitation phenomenon. Under the super cavitation condition, due to the formation of large number of cavities at inlet pressure beyond 5 bar, the cavities coalesce with each other and are carried away with the flowing liquid without collapse. According to Fig. 9, as the inlet pressure increases, cavitation zone would increase that indicate the CFD simulation can't see the super cavitation process.

It is also worth mentioning that the extent of decolorization is continuously improved with reaction time proceeding.

4.4. Performance comparison of Venturi and orifice

Details of the cavitating devices, the optimum inlet pressure, cavitation number and the decolorization rate for different geometries are given in Table 7. Two important parameters α and β were used to characterize the geometry of orifice plate. Parameter α is defined as the ratio of total perimeter of holes to the total area of the opening and β is defined as the ratio of total flow area to the cross sectional area of the pipe. All geometries have the same β equal to 0.0178. According to Table 7, the decolorization rate of orifice plate increased with an increase in the value of α. The orifice plates having larger number of holes and longer total perimeter of holes could enhance the decolorization rate of orifice plates.

Based on the CR decolorization study, the maximum yield is obtained at HC inlet pressure of 5 bar for the Venturi. While it has been observed at 6 bar for the OP1 and OP3 orifice. The maximum decolorization rate was obtained in case of Venturi, whereas lowest decolorization rate was exhibited by OP1 (single hole) orifice plate. About 38.8% decolorization was obtained in the case of Venturi, whereas 26.2% and 11.5% decolorization was gained by OP4 (33 holes) orifice and OP1 (single hole) orifice respectively in 60 min at optimum inlet pressure. It is concluded that Venturi posed an improved performance in comparison with the orifice plates. It could be due to the smooth convergent and divergent sections that avoid rapid cavity collapse and increases the cavity life hence the bubbles have enough time to reach their maximum size unlike the orifice plate. In addition, the Venturi generates higher cavitational events at the throat as well as the usage of lower amount of energy. Saharan et al. [30] have proved that in case of Venturies, the cavitation number was lower than the orifice for the same pressure drop across the cavitating device, and hence Venturies generate higher number of cavities than orifice that leads to higher decolorization rates.

Fig. 10 illustrates the change in decolorization with time for the three cavitating devices at their optimized inlet pressure. Fig. 11 depicts the change in decolorization with different inlet pressure for four types of

Table 7
Effect of geometrical parameters on decolorization of Congo red.

Cavitating device	Number of holes	Diameter of holes	Perimeter of holes	α (mm^{-1})	Decolorization%	inlet optimum pressure (bar)	C_v
OP1	1	4	12.56	1	11.55	6	0.11
OP2	13	1.1	44.9	3.64	17.36	5	0.097
OP3	25	0.8	62.8	5	25.1	6	0.24
OP4	33	0.69	71.5	5.8	26.2	5	0.13
Venturi	1	4	12.56	1	38.8	5	0.12

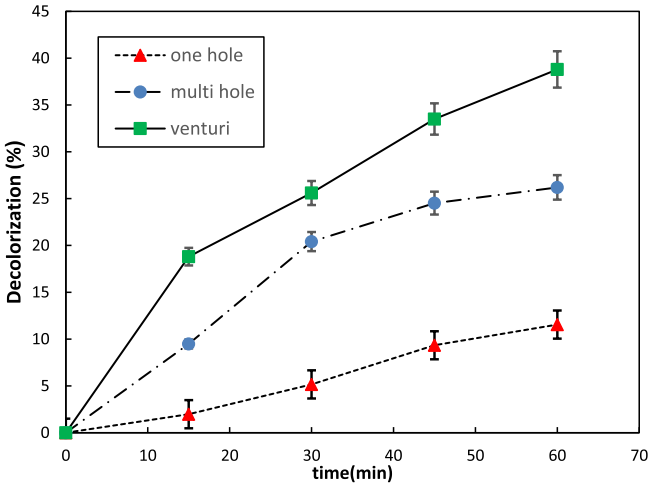

Fig. 10. Decolorization rate of Congo red in three different cavitating device.

orifice plates and Venturi. As per the observation, decolorization improved subsequent to increase in the inlet pressure reaching a maximum. Thereafter decay in decolorization has appeared that could be attributed to the super cavitation phenomenon [15].

The decolorization kinetics of hydrodynamic cavitation follows a first order law, given by Eq. (15):

$$\ln\left(\frac{C_0}{C}\right) = k^*t \tag{15}$$

where C is the concentration of Congo red at time t, C_0 is the initial concentration, and k is the 1st order rate constant. Many researches have also indicate that degradation of organic pollutants using HC follows a first order kinetic [4,18]. Fig. 12 demonstrates the plot of the $\ln(C_0/C)$ vs time (t). This plot is a straight line passing through the origin, that confirms the decolorization of Congo red obeys a first order reaction kinetics. The rate constants are reported at Table 8. According to the

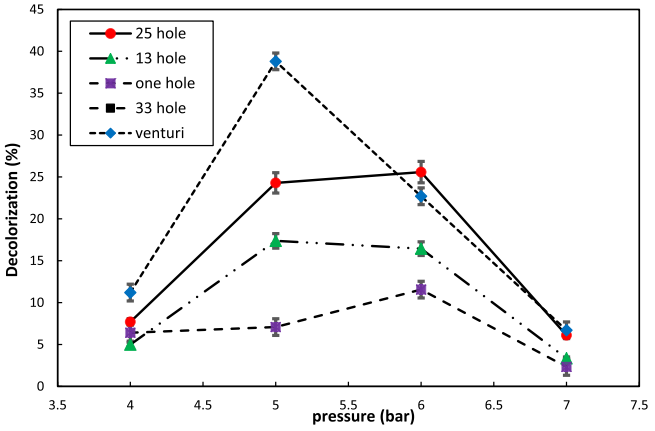

Fig. 11. Decolorization rate in the various inlet pressure using different cavitating devices.

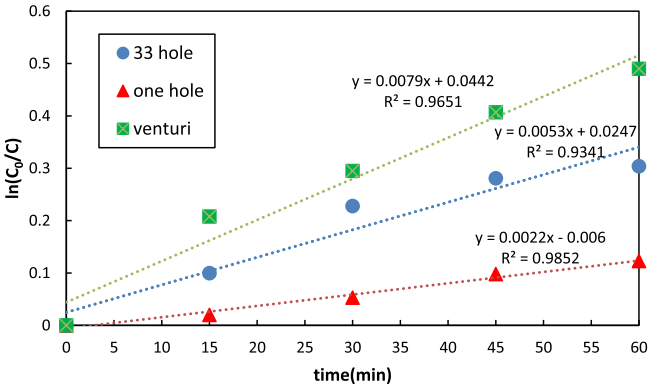

Fig. 12. First order decolorization of Congo red at three cavitating devices.

results, the venturi exhibited the maximum decolorization rate constant.

5. Conclusions

In the present study, effect of operational and geometrical parameters on performance of Venturi reactor was investigated utilizing CFD simulation. The following main conclusions can be deducted from the present work.

- Box-Behnken design (BBD) was employed to determine the optimal geometric parameters for Venturi, based on the length of cavitation zone in downstream section.
- Each of the proposed geometries has been simulated through CFD approach, the flow through Venturi reactor was numerically simulated by taking steady flow condition in standard k-ε turbulent scheme and mixture model for multiphase flow.
- According to the modelling findings, maximum cavitation zone was obtained in a Venturi with inlet angle of 22.7°, length of throat 4 mm and outlet angle of 6.5°. The results show that the three geometrical parameters are related to each other and the divergence angle is the most effective parameter that affects the cavitation zone whereas the convergence angle is the least significant parameter.
- In order to validate the performance of optimized Venturi, cavitation length was evaluated experimentally. The pressure contour resulting from simulation of optimized Venturi has been matched with imaging evidence of cavitation zone forming in the experimental section.
- Maximum decolorization of CR of 38.8% was appeared to be at optimum inlet pressure of 5 bar and cavitation number of 0.12.
- The experimental study shows that increase in the inlet pressure up to 5 bar results in an increase in the extent of decolorization of CR. At operating Venturi inlet pressure of higher than 5 bar correspond to

Table 8
Decolorization rate constant, k for the cavitating devices.

Cavitating devices	First order constant (min^{-1})*10^{-3}
Venturi	7.9
OP4 (33 holes)	5.3
OP1 (One hole)	2.2

the cavitation number (Cv) of 0.12, super cavitation occurs that leads to decreased rate of Congo red decolorization.

- 26.2% and 11.55% decolorization was obtained by 33 holes orifice and single hole orifice respectively in 60 min at optimum inlet pressure which these decolorization was compared with optimized Venturi. It has maximum decolorization rate constant (7.9×10^{-3} min^{-1}) in comparison with orifice plates.

CRediT authorship contribution statement

Zahra Abbas-Shiroodi: Software, Writing - original draft, Visualization, Investigation. **Mohammad-Taghi Sadeghi:** Conceptualization, Methodology, Supervision, Writing - review & editing. **Soroush Baradaran:** Software, Data curation, Validation.

Declaration of Competing Interest

The authors declare that they have no known competing financial interests or personal relationships that could have appeared to influence the work reported in this paper.

References

[1] P.R. Gogate, A.B. Pandit, Hydrodynamic cavitation reactors: a state of the art review, 2001. doi: 10.1515/REVCE.2001.17.1.1.

[2] S. Rajoriya, J. Carpenter, V.K. Saharan, A.B. Pandit, Hydrodynamic cavitation: an advanced oxidation process for the degradation of bio-refractory pollutants, Rev. Chem. Eng. 32 (2016) 379–411, https://doi.org/10.1515/revce-2015-0075.

[3] J. Ozonek, Application of hydrodynamic cavitation in environmental engineering, 2012. doi: 10.1201/b11825.

[4] S. Rajoriya, S. Bargole, V.K. Saharan, Degradation of reactive blue 13 using hydrodynamic cavitation: Effect of geometrical parameters and different oxidizing additives, Ultrason. Sonochem. 37 (2017) 192–202, https://doi.org/10.1016/j.ultsonch.2017.01.005.

[5] G. Mancuso, M. Langone, G. Andreottola, L. Bruni, Effects of hydrodynamic cavitation, low-level thermal and low-level alkaline pre-treatments on sludge solubilisation, Ultrason. Sonochem. 59 (2019), 104750, https://doi.org/10.1016/j.ultsonch.2019.104750.

[6] B. Kompare, B. Širok, M. Zupanc, T. Kosjek, M. Petkovšek, E. Heath, Shear-induced hydrodynamic cavitation as a tool for pharmaceutical micropollutants removal from urban wastewater, Ultrason. Sonochem. 21 (2014) 1213–1221, https://doi.org/10.1016/j.ultsonch.2013.10.025.

[7] P. Rudolf, M. Hudec, B. Mar, High-pressure jet-induced hydrodynamic cavitation as a pre-treatment step for avoiding cyanobacterial contamination during water purifications a, 255 (2020). doi: 10.1016/j.jenvman.2019.109862.

[8] K.K. Jyoti, A.B. Pandit, Water disinfection by acoustic and hydrodynamic cavitation, 7 (2001) 201–212.

[9] N. Ra, Efficient inactivation of MS-2 virus in water by hydrodynamic cavitation, 124 (2017) 465–471. doi: 10.1016/j.watres.2017.07.077.

[10] G. Mancuso, M. Langone, G. Andreottola, A critical review of the current technologies in wastewater treatment plants by using hydrodynamic cavitation process: principles and applications, J. Environ. Heal. Sci. Eng. 18 (2020) 311–333, https://doi.org/10.1007/s40201-020-00444-5.

[11] A. Przyjazny, G. Boczkaj, Wastewater treatment by means of advanced oxidation processes based on cavitation – a review, 338 (2018) 599–627. doi: 10.1016/j.cej.2018.01.049.

[12] S. Baradaran, M.T. Sadeghi, Intensification of diesel oxidative desulfurization via hydrodynamic cavitation, Ultrason. Sonochem. 58 (2019), 104698, https://doi.org/10.1016/j.ultsonch.2019.104698.

[13] S. Baradaran, M.T. Sadeghi, Desulfurization of non-hydrotreated kerosene using hydrodynamic cavitation assisted oxidative desulfurization (HCAOD) process, J. Environ. Chem. Eng. 8 (2020), 103832, https://doi.org/10.1016/j.jece.2020.103832.

[14] V.K. Saharan, M.P. Badve, A.B. Pandit, Degradation of Reactive Red 120 dye using hydrodynamic cavitation, Chem. Eng. J. 178 (2011) 100–107, https://doi.org/10.1016/j.cej.2011.10.018.

[15] S. Baradaran, M.T. Sadeghi, Coomassie Brilliant Blue (CBB) degradation using hydrodynamic cavitation, hydrogen peroxide and activated persulfate (HC-H 2 O 2 -KPS) combined process, Chem. Eng. Process. Process Intensification. 145 (2019), 107674, https://doi.org/10.1016/j.cep.2019.107674.

[16] Z. Askarniya, M.T. Sadeghi, S. Baradaran, Decolorization of Congo red via hydrodynamic cavitation in combination with Fenton's reagent, Chem. Eng. Processing: Process Intensification 150 (2020).

[17] M.M. Gore, V.K. Saharan, D.V. Pinjari, P.V. Chavan, A.B. Pandit, Degradation of reactive orange 4 dye using hydrodynamic cavitation based hybrid techniques, Ultrason. Sonochem. 21 (2014) 1075–1082, https://doi.org/10.1016/j.ultsonch.2013.11.015.

[18] S. Raut-Jadhav, V.K. Saharan, D.V. Pinjari, D.R. Saini, S.H. Sonawane, A.B. Pandit, Intensification of degradation of imidacloprid in aqueous solutions by combination of hydrodynamic cavitation with various advanced oxidation processes (AOPs), J. Environ. Chem. Eng. 1 (2013) 850–857, https://doi.org/10.1016/j.jece.2013.07.029.

[19] S. Raut-Jadhav, D. Saini, S. Sonawane, A. Pandit, Effect of process intensifying parameters on the hydrodynamic cavitation based degradation of commercial pesticide (methomyl) in the aqueous solution, Ultrason. Sonochem. 28 (2015) 283–293, https://doi.org/10.1016/j.ultsonch.2015.08.004.

[20] V.K. Saharan, A.B. Pandit, P.S. Satish Kumar, S. Anandan, Hydrodynamic cavitation as an advanced oxidation technique for the degradation of Acid Red 88 dye, Ind. Eng. Chem. Res. 51 (2012) 1981–1989, https://doi.org/10.1021/ie200249k.

[21] H. Ma, M. Wang, R. Yang, W. Wang, J. Zhao, Radiation degradation of Congo Red in aqueous solution, 68 (2007) 1098–1104. doi: 10.1016/j.chemosphere.2007.01.067.

[22] C.S.E. Berghahn, V.I.C.E. Granada, Biodegradation potential of Citrobacter cultures for the removal of amaranth and congo red azo dyes, Int. J. Environ. Sci. Technol. (2019), https://doi.org/10.1007/s13762-019-02274-x.

[23] P.V. Nidheesh, R. Gandhimathi, Degradation of dyes from aqueous solution by Fenton processes : a review, (2013). doi: 10.1007/s11356-012-1385-z.

[24] G. Oros, E. Forgacs, T. Cserha, Removal of synthetic dyes from wastewaters : a review, 30 (2004) 953–971. doi: 10.1016/j.envint.2004.02.001.

[25] M. Khadhraoui, H. Trabelsi, M. Ksibi, S. Bouguerra, B. Elleuch, Discoloration and detoxicification of a Congo red dye solution by means of ozone treatment for a possible water reuse, 161 (2009) 974–981. doi: 10.1016/j.jhazmat.2008.04.060.

[26] E. Burzio, F. Bersani, G.C.A. Caridi, R. Vesipa, L. Ridol, C. Manes, Water disinfection by orifice-induced hydrodynamic cavitation, Ultrason. Sonochem. 60 (2020), https://doi.org/10.1016/j.ultsonch.2019.104740.

[27] B. Mar, P. Rudolf, Synergistic effects of trace concentrations of hydrogen peroxide used in a novel hydrodynamic cavitation device allows for selective removal of cyanobacteria, 382 (2020). doi: 10.1016/j.cej.2019.122383.

[28] G. Mancuso, M. Langone, G. Andreottola, Ultrasonics Sonochemistry A swirling jet-induced cavitation to increase activated sludge solubilisation and aerobic sludge biodegradability, Ultrason. Sonochem. 35 (2017) 489–501, https://doi.org/10.1016/j.ultsonch.2016.11.006.

[29] G. Mancuso, M. Langone, M. Laezza, G. Andreottola, Decolourization of Rhodamine B: a swirling jet-induced cavitation combined with NaOCl, Ultrason. Sonochem. 32 (2016) 18–30, https://doi.org/10.1016/j.ultsonch.2016.01.040.

[30] V.K. Saharan, M.A. Rizwani, A.A. Malani, A.B. Pandit, Effect of geometry of hydrodynamically cavitating device on degradation of orange-G, Ultrason. Sonochem. 20 (2013) 345–353, https://doi.org/10.1016/j.ultsonch.2012.08.011.

[31] A.A. Pradhan, P.R. Gogate, Removal of p-nitrophenol using hydrodynamic cavitation and Fenton chemistry at pilot scale operation, Chem. Eng. J. 156 (2010) 77–82, https://doi.org/10.1016/j.cej.2009.09.042.

[32] M.P. Badve, M.N. Bhagat, A.B. Pandit, Microbial disinfection of seawater using hydrodynamic cavitation, Sep. Purif. Technol. 151 (2015) 31–38, https://doi.org/10.1016/j.seppur.2015.07.020.

[33] T.A. Bashir, A.G. Soni, A.V. Mahulkar, A.B. Pandit, The CFD driven optimisation of a modified venturi for cavitational activity, Can. J. Chem. Eng. 89 (2011) 1366–1375, https://doi.org/10.1002/cjce.20500.

[34] G. Mancuso, Experimental and numerical investigation on performance of a swirling jet reactor, Ultrason. Sonochem. 49 (2018) 241–248, https://doi.org/10.1016/j.ultsonch.2018.08.011.

[35] S.L.C. Ferreira, R.E. Bruns, H.S. Ferreira, G.D. Matos, J.M. David, G.C. Brandão, E. G.P. da Silva, L.A. Portugal, P.S. dos Reis, A.S. Souza, W.N.L. dos Santos, Box-Behnken design: an alternative for the optimization of analytical methods, Anal. Chim. Acta 597 (2007) 179–186, https://doi.org/10.1016/j.aca.2007.07.011.

[36] D.C. Montgomery, Design and Analysis of Experiments: Eight Edition, 2012. http://cataleg.uab.cat/record=b1764873~S1*cat.

[37] R. Field, Introduction, 18 (2002).

[38] A.K. Singhal, M.M. Athavale, H. Li, Y. Jiang, Mathematical basis and validation of the full cavitation model, J. Fluids Eng. 124 (2002) 617, https://doi.org/10.1115/1.1486223.

[39] V.K. Kuldeep, Saharan, Computational study of different venturi and orifice type hydrodynamic cavitating devices, J. Hydrodyn. 28 (2016) 293–305, https://doi.org/10.1016/S1001-6058(16)60631-5.

[40] J. Carpenter, V. Kumar, Study of Cavity dynamics in a Hydrodynamic Cavitation Reactor, 1 (2017) 37–43.

[41] J. Carpenter, M. Badve, S. Rajoriya, S. George, V.K. Saharan, A.B. Pandit, Hydrodynamic cavitation: an emerging technology for the intensification of various chemical and physical processes in a chemical process industry, Rev. Chem. Eng. 33 (2017) 433–468, https://doi.org/10.1515/revce-2016-0032.

[42] C.E. Brennen, Cavitation and Bubble Dynamics (Oxford Engineering Science Series), 1995. http://www.amazon.com/exec/obidos/redirect?tag=citeulike07-20&path=ASIN/0195094093.

[43] S. Raut-Jadhav, V.K. Saharan, D. Pinjari, S. Sonawane, D. Saini, A. Pandit, Synergetic effect of combination of AOP's (hydrodynamic cavitation and H 2 O 2) on the degradation of neonicotinoid class of insecticide, J. Hazard. Mater. 261 (2013) 139–147, https://doi.org/10.1016/j.jhazmat.2013.07.012.